

Inhibition of PI3K and Hedgehog Signaling Pathway Inhibits Hypoxia-Induced Vasculogenic Mimicry Formation in Ovarian Cancer Stem Cells

Jun Liang, Yun Bai, Huan Zhao

Department of Obstetrics and Gynecology, Hebei Medical University Third Hospital, Hebei Province, China

Background: Inhibition of the Hedgehog and phosphatidylinositol 3-kinase/protein kinase B (PI3K/AKT) signaling pathways has been shown to suppress tumor proliferation and stem cell activity. However, the precise role of these pathways in vasculogenic mimicry (VM) of ovarian cancer stem cells (OCSCs) remains unclear.

Aims: To investigate the roles of the PI3K/AKT and Hedgehog signaling pathways in VM formation and the underlying mechanisms in OCSCs.

Study Design: *In vitro* and *in vivo* experimental model.

Methods: OCSCs were induced through serum-free culture of SK-OV-3. Hypoxia-inducible factor-1 α (HIF-1 α) knockdown was achieved by transfection with sh-HIF-1 α . Cells were treated with the PI3K agonist 740 Y-P, the PI3K inhibitor LY294002, the Hedgehog agonist purmorphamine, and the Hedgehog inhibitor cyclopamine under hypoxic conditions. Expression of HIF-1 α , epithelial-to-endothelial transition (EET) markers, and components of the PI3K and Hedgehog pathways was analyzed using immunofluorescence and Western blotting. VM capacity was assessed using a Matrigel three-dimensional (3D) culture assay. Cell proliferation

and invasion were evaluated by MTS, EdU, and Transwell assays. VM formation was further examined in an OCSC xenograft model.

Results: OCSCs accounted for more than 85% of seventh-generation SK-OV-3 cells cultured under serum-free conditions. Hypoxia markedly increased HIF-1 α expression, which activated the PI3K and Hedgehog signaling pathways. HIF-1 α knockdown suppressed activation of these pathways. Treatment with LY294002 and cyclopamine, as well as HIF-1 α knockdown, inhibited hypoxia-induced upregulation of N-cadherin and VE-cadherin, as well as the formation of branching points and 3D channels. Moreover, both LY294002 and cyclopamine significantly reduced cell proliferation, invasion, and VM formation *in vitro* and *in vivo*.

Conclusion: HIF-1 α knockdown inhibits activation of the PI3K and Hedgehog signaling pathways, thereby reducing EET and VM formation in hypoxia-induced OCSCs.

INTRODUCTION

Ovarian cancer (OC) is associated with a high mortality rate¹ and ranks first among malignancies of the female reproductive system. According to the International Cancer Research Center, more than 200,000 women worldwide died of OC in 2020.² Because the ovaries are located deep within the pelvic cavity, approximately 80% of cases are diagnosed at an advanced stage, resulting in a 5-year survival rate of only about 40%.³ Traditional treatment mainly consists of surgery combined with chemotherapy, supplemented by targeted therapy and immunotherapy. Although progress has been made in recent years, many patients achieve clinical remission after initial treatment, yet up to 70% experience disease recurrence within 2-3 years.⁴ In light of this, there is an urgent need to explore and develop novel therapeutic approaches for OC.

Cancer stem cells (CSCs) are a subset of tumor cells with stem cell-like properties, including self-renewal, unlimited proliferation, and multipotent differentiation.^{5,6} CSCs promote OC invasion and metastasis through various mechanisms and influence cellular behavior within the tumor microenvironment, which is closely associated with patient prognosis.^{7,8} Studies have shown that CSCs possess strong differentiation potential and contribute to tumor angiogenesis, thereby supporting tumor growth, invasion, and metastasis. Vasculogenic mimicry (VM) represents another mechanism of tumor vascularization in addition to traditional angiogenesis. Unlike endothelial cell-dependent angiogenesis, VM forms vessel-like networks that provides an alternative blood supply to tumors.⁹ VM is closely linked to OC metastasis and may represent an important therapeutic target.¹⁰ Furthermore, VM can promote the growth of ovarian cancer stem cells (OCSCs).¹¹ Therefore, elucidating



Corresponding author: Jun Liang, Department of Obstetrics and Gynecology, Hebei Medical University Third Hospital, Hebei Province, China

e-mail: L13582026972LJ@hotmail.com

Received: July 29, 2025 **Accepted:** August 20, 2025 **Available Online Date:** 01.09.2025 • **DOI:** 10.4274/balkanmedj.galenos.2025.2025-7-262

Available at www.balkanmedicaljournal.org

ORCID iDs of the authors: J.L. 0009-0001-4169-4104; Y.B. 0000-0003-3222-5557; H.Z. 0009-0003-1802-1600.

Cite this article as: Liang J, Bai Y, Zhao H. Inhibition of PI3K and Hedgehog Signaling Pathway Inhibits Hypoxia-Induced Vasculogenic Mimicry Formation in Ovarian Cancer Stem Cells. Balkan Med J; 2025; 42(5):440-51.

Copyright@Author(s) - Available online at <http://balkanmedicaljournal.org>

the mechanisms underlying VM formation in OCSCs is of great significance for identifying novel therapeutic targets for OC.

The phosphatidylinositol 3-kinase/protein kinase B (PI3K/AKT) pathway is associated with proliferation, adhesion, migration, and other malignant biological behaviors of tumor cells. This signaling cascade also contributes to the occurrence and progression of OC.^{12,13} Existing evidence suggests that PI3K/AKT signaling is involved in the mechanism of VM formation in tumor tissues. Inhibition of the PI3K/AKT pathway significantly reduces vascular endothelial (VE)-cadherin and matrix metalloproteinase-2 (MMP2) expression, thereby impeding VM network formation.¹⁴ Conversely, activation of this pathway promotes breast cancer growth and VM.¹⁵ Thrombospondin-2 has also been shown to regulate tumor VM by activating the PI3K/AKT pathway.¹⁶ The Hedgehog signaling pathway likewise plays an important role in OC progression. Variations in the expression of its key regulatory factors may be associated with histopathological type, grade, and differentiation of OC.¹⁷ Moreover, studies have demonstrated that Galectin-1 can promote VM in gastric adenocarcinoma via the Hedgehog pathway.¹⁸ Collectively, these findings suggest that the PI3K/AKT and Hedgehog pathways may represent promising therapeutic targets for inhibiting VM in OCSCs.

In this study, sloan-kettering ovarian carcinoma 3 (SK-OV-3) cells were subcultured using the serum-free suspension culture method, and cell spheres with stem-like properties of OCSCs were isolated. We investigated the effects of the PI3K/AKT and Hedgehog pathways on VM formation in hypoxia-induced OCSCs and explored the underlying mechanisms at the cellular level, with further validation *in vivo*, aiming to identify new therapeutic targets for OC.

MATERIALS AND METHODS

Cell culture

Human OC SK-OV-3 cells were purchased from Saibaikang Biotechnology Co., Ltd. (iCell-h195, Shanghai, China). Cells were cultured in DMEM supplemented with 10% fetal bovine serum (FBS; G8002, Servicebio, Wuhan, China) and 1% penicillin-streptomycin (G4015, Servicebio) at 37 °C in a humidified incubator containing 5% CO₂ (WCI-1200, WIGGENS, Germany). Cultures were passaged every 2-3 days.

Induction of SK-OV-3 OCSCs by serum-free culture

SK-OV-3 cells in good growth condition were dissociated with 0.25% trypsin-EDTA and cultured in serum-free DMEM/F12 medium containing 20 ng/mL epidermal growth factor, 10 ng/mL basic fibroblast growth factor, 2% B27 supplement, and 5 mg/mL recombinant human insulin.¹⁹ Under these conditions, the cells formed non-adherent spheres. For serial passage, spheres were centrifuged, digested with trypsin, and recultured in serum-free medium. The medium was changed every other day, and low-speed centrifugation for 5 min was performed to remove dead cell debris. Cells from the first and seventh generations were collected, and the growth of suspended cell spheres was observed and photographed.

Identification of SK-OV-3 OCSCs

A total of 1×10^6 SK-OV-3 cells were washed with 500-µL phosphate buffered saline (PBS)/EDTA/BSA solution and digested with trypsin (G4013, Servicebio). The isolated cells were resuspended in PBS/EDTA/BSA solution, and 2 µL of human FcR blocking reagent was added. The suspension was incubated at 4 °C for 10 min, followed by the addition of 1-µg anti-CD44-PE (BJ18, BioLegend, California, USA) and anti-CD24-FITC (32D12, BioLegend) antibodies. The mixture was gently mixed and incubated at 4 °C for 10 min in the dark. Cells were then fixed in PBS containing 1% paraformaldehyde and analyzed by flow cytometry (BD Influx, BD Biosciences, Franklin Lakes, NJ, USA).

Cell transfection and treatment

SK-OV-3 OCSCs were prepared as a cell suspension and seeded into 6-well plates at a density of 3×10^5 cells per well and then cultured in serum-free medium. When cell confluence reached approximately 60%, hypoxia-inducible factor-1α (HIF-1α), sh-HIF-1α, and their respective negative controls (Vector and sh-NC) were transfected. Lipofectamine™ 2000 (200 µL; 11668019, Invitrogen, California, USA) was used for transfection according to the manufacturer's protocol. After 6 h, the medium was replaced with serum-containing medium. Cells were harvested 48 h later for detection of HIF-1α protein levels. Vector, HIF-1α, sh-NC, and sh-HIF-1α plasmids were purchased from GEMMA Biotechnology Co., Ltd. (Suzhou, China).

Transfected or untransfected SK-OV-3 OCSCs were then treated with the PI3K pathway agonist 740 Y-P (25 mg/mL, S7865, Selleck, Shanghai, China) or inhibitor LY294002 (30 µM, S1737, Beyotime, Shanghai, China), and the Hedgehog pathway agonist purmorphamine (1 µM, SF6822, Beyotime) or inhibitor cyclopamine (20 µM, S1146, Selleck). To mimic hypoxic conditions, cells were treated with cobalt chloride (CoCl₂, 150 µM; 232696, Sigma, Shanghai, China) for 0, 3, 6, 12, 24, or 48 h.²⁰

Immunofluorescence

SK-OV-3 OCSCs (1×10^5 cells/well) were seeded onto sterile coverslips. After overnight adherence, cells were treated with CoCl₂ and cultured for 0, 3, 6, 12, 24, or 48 h. Cells were then fixed with methanol, permeabilized with PBS containing 0.1% Triton X-100 for 15 min, and blocked with phosphate buffered saline tween at room temperature for 30 min. Cells were incubated with anti-HIF-1α antibody (ab51608, Abcam, Cambridge, UK) at 4 °C overnight, followed by incubation with fluorescent secondary antibody (GB25303, Servicebio) in the dark for 1 h. Slides were mounted with a fluorescence mounting medium containing 4 ',6-diamidino-2-phenylindole (DAPI) (G1401, Servicebio) and air-dried. Images were captured using a confocal microscope (FV3000, Olympus, Tokyo, Japan). Fluorescence intensity was independently evaluated by two pathologists in a blinded manner. During sample collection, only sample numbers were available to the operator, with no access to grouping information. Data measurement and image storage were performed using coded identifiers to prevent exposure of experimental conditions.

Three-dimensional (3D) matrigel culture assay

Matrigel was mixed with DMEM at a 1:1 ratio, evenly spread into precooled wells of a 96-well plate, and allowed to solidify for 2 h. A 100- μ L suspension of SK-OV-3 OCSCs (1×10^7 cells/mL) was added to each well and cultured for 24 h. VM formation was observed under a microscope. Images were captured from five randomly selected fields (upper, middle, lower, left, and right). The number of branch points and three-dimensional (3D) channels was counted, and the average value was calculated. Evaluation was performed independently by two pathologists in a blinded manner.

MTS assay

Following treatment, SK-OV-3 OCSCs were incubated with 20 μ L of MTS reagent (G5421, Promega, Madison, WI, USA) for 1 h. Absorbance was then measured at 490 nm using a microplate reader (SpectraMax i3x, Molecular Devices, San Jose, CA, USA).

EdU assay

Treated SK-OV-3 OCSCs were incubated with 50- μ M EdU reagent (C0071L, Beyotime, Shanghai, China) for 2 h. After the culture medium was removed, cells were fixed in 1-mL fixative solution for 15 min, permeabilized with 1-mL permeabilization solution for 15 min, and then incubated with 0.5-mL reaction solution for 30 min. After washing, nuclei were counterstained with DAPI. Fluorescence microscopy was used for observation and analysis. EdU-positive cells were counted independently by two pathologists in a blinded manner.

Transwell invasion assay

SK-OV-3 OCSCs were seeded into the upper chamber of a Transwell insert (354234, Corning, New York, United States) precoated with Matrigel, at a density of 1×10^5 cells per chamber in 200- μ L serum-free medium. The lower chamber contained medium supplemented with 5% serum. After 24 h of culture, non-invading cells in the upper chamber were removed, and invading cells were fixed with 4% paraformaldehyde for 15 min and stained with 0.1% crystal violet for 20 min. Cells in five non-overlapping fields were counted under a fluorescence microscope, and the average value was calculated. Cell counts were performed independently by two pathologists in a blinded manner.

Xenograft nude mouse model

Twenty-five female BALB/c Nu/Nu mice (6 weeks old, 15-20 g) were purchased from Ziyuan Experimental Animal Technology Co., Ltd. (Hangzhou, China). The mice were housed under specific pathogen-free conditions (25 °C, 60% humidity) with free access to food and water. All animal experiments were approved by the Ethics Committee of the Third Hospital of Hebei Medical University (approval number: 2025-083-1, date: 12.06. 2025).

The mice were randomly assigned (n = 5 per group) into the following groups using the random number table method: control, 740 Y-P group, LY294002, purmorphamine, and cyclopamine. OCSCs isolated from the SK-OV-3 cell line were injected subcutaneously into the dorsal flank to establish the xenograft tumor model.²¹ Mice in the control group received intraperitoneal injections of normal saline,

while the treatment groups received intraperitoneal injections of 740 Y-P (20 mg/kg), LY294002 (50 mg/kg), purmorphamine (10 mg/kg), or cyclopamine (10 mg/kg), administered twice weekly. Tumor growth was monitored using a small animal *in vivo* imaging system (IVIS® Lumina III, PerkinElmer, Massachusetts, USA) on days 7, 14, 21, and 28. After 4 weeks, the mice were euthanized by anesthesia, and the tumors were excised and weighed. Each tumor was divided into two parts: one was fixed in 4% paraformaldehyde, and the other was stored at -80 °C for subsequent experiments. To minimize experimental bias, the random number table method was used throughout the study for data processing and measurement. In addition, all animal experiments were conducted under blinded conditions: (1) animal allocation, researchers were unaware of group assignments; (2) experimental procedures, animal handlers and researchers were blinded to the grouping; and (3) outcome evaluation and data analysis, the investigators responsible for evaluating and analyzing results were blinded to the grouping.

Immunohistochemistry

Formalin-fixed tumor tissues were paraffin-embedded and sectioned at 4- μ m thickness. Sections were baked at 60 °C, deparaffinized in a xylene gradient, rehydrated in an ethanol gradient, subjected to antigen retrieval, and blocked for endogenous peroxidase activity. They were then incubated overnight at 4 °C with primary antibodies against Ki-67 (ab16667, Abcam) and CD31 (ab281583, Abcam). The next day, sections were incubated with an appropriate secondary antibody for 20 min, followed by DAB staining for 5 min, hematoxylin counterstaining, dehydration, clearing, and mounting with neutral gum. Ki-67-positive nuclei appeared yellow or brown. Five randomly selected, non-overlapping high-power fields were evaluated, and images were captured using a fluorescence microscope (Odyssey, Laikuo Biotechnology Co., Ltd., Beijing, China).

PAS staining

Tissue sections were incubated in sodium periodate solution for 15 min, followed by incubation with Schiff reagent in the dark for 15 min. Nuclei were counterstained with hematoxylin for 20 s and rinsed with running water. The sections were then dehydrated in ethanol, cleared in xylene for 5 min, air-dried at room temperature, and mounted with neutral gum. The sections were observed under a light microscope (E200, Nikon, Tokyo, Japan). Positive PAS staining was used to identify VM.

Western blot

Total protein from SK-OV-3 OCSCs and xenograft tumor tissues was extracted using RIPA lysis buffer (G2002, Servicebio), and protein concentration was determined with a BCA assay (G2026, Servicebio). Equal amounts of protein (15 μ g per sample) were separated by 10% SDS-PAGE and transferred to PVDF membranes (G6047, Servicebio) using the wet transfer method. Membranes were blocked with 5% skim milk for 90 min and incubated overnight at 4 °C with primary antibodies (ab97051, Abcam) for 1 h, protein bands were detected using an enhanced chemiluminescence substrate (ECL, A38556, Thermo Fisher Scientific, Massachusetts, USA) and imaged with a chemiluminescence imaging system (ChemiDoc XRS+, Bio-Rad). Band intensities were quantified using Image J software, and

statistical analyses were performed.

The following primary antibodies were used: HIF-1 α (ab51608, Abcam), PI3K (4292, Cell Signaling Technology), p-PI3K (17366, Cell Signaling Technology), AKT (ab314110, Abcam), p-AKT (ab38449, Abcam), Smoothened (Smo, ab235183, Abcam), Sonic Hedgehog (SHH, ab135240, Abcam), Gli1 (ab289368, Abcam), E-cadherin (ab227639, Abcam), N-cadherin (ab245117, Abcam), VE-cadherin (ab313632, Abcam), Ki-67 (ab16667, Abcam), MMP2 (ab181286, Abcam), and MMP9 (ab137867, Abcam).

Statistical analysis

Biological replicates were obtained from independent samples. Data are presented as the mean \pm standard deviation from three independent experiments and were analyzed using GraphPad Prism 9.0 (GraphPad Software, San Diego, CA, USA). Normality was assessed with the Shapiro-Wilk test, and homogeneity of variance with the Levene test. Comparisons between the two groups were performed using the Student's t-test. For multiple-group comparisons, one-way ANOVA followed by Tukey's honest significant difference post-hoc test was applied when data did not meet assumptions of normality and homogeneity assumption. If assumptions were not met, the Kruskal-Wallis test with Dunn's post hoc test was used. Tumor growth curves were analyzed using repeated-measures ANOVA. All tests were two-tailed, with statistical significance set at $p < 0.05$ and a 95% confidence interval.

RESULTS

Identification of OCSCs

During the induction of SK-OV-3 cells to form OCSCs in serum-free medium, most cells settled at the bottom of the culture plate, with a few showing adherent growth. After about 24 h, most cells died, leaving only a small number of surviving cells in suspension. By 2-4 days, small suspended spheres consisting of three to eight cells of uniform size and with defined refractive index were observed. By 5-7 days, the number and size of spheres increased, with dozens of cells forming tightly connected clusters with indistinct boundaries and enhanced refraction. With successive passages, both the number and volume of suspended spheres further increased (Figure 1a). The CD44 $^+$ CD24 $^-$ phenotype is a recognized marker for CSC identification.²⁰ In the first generation of serum-free cultured SK-OV-3 cells, this phenotype was almost absent, whereas it accounted for 85.76 \pm 1.64% in the seventh generation (Figure 1b). These findings indicate that SK-OV-3 OCSCs were successfully induced by serum-free culture.

Hypoxia induces HIF-1 α expression of SK-OV-3 OCSCs

Because hypoxia is closely associated with the VM process, and HIF-1 α is a key marker of VM formation²², CoCl₂ was used to mimic a hypoxic environment. SK-OV-3 OCSCs were cultured under hypoxia for 0, 3, 6, 12, 24, and 48 h. The fluorescence intensity of HIF-1 α increased significantly after 12 h of hypoxia, rising by 1.32-, 2.06-, and 1.63-fold at 12, 24, and 48 h, respectively (12 h, $p = 0.023$; 24 and 48 h, $p < 0.001$; Figures 2a, b). Western blot analysis also showed a significant increase in HIF-1 α protein expressions at 24 and 48 h, with levels rising by 1.33-, 2.13-, and 1.74-fold, respectively (12 h, $p = 0.028$; 24 and 48 h, $p < 0.001$; Figure 2c). Notably, both fluorescence intensity and protein expression peaked at 24 h of

hypoxia. Based on these findings, 24 h of hypoxia was selected for subsequent experiments. Together with the OCSC identification results, which showed that 80%-90% of SK-OV-3 OCSCs displayed the CD44 $^+$ CD24 $^-$ phenotype, these data confirm that SK-OV-3 OCSCs exhibit a strong ability to form VM.

Knockdown of HIF-1 α suppresses activation of the PI3K and Hedgehog signaling pathways under hypoxia

After 24 h of hypoxia in SK-OV-3 OCSCs, expression of p-PI3K (1.60-fold, $p < 0.001$) and p-AKT (1.71-fold, $p < 0.001$) increased significantly, indicating activation of the PI3K pathway. Similarly, the expression of Smo (1.51-fold), SHH (1.69-fold), and Gli1 (3.65-fold) proteins was markedly elevated, suggesting activation of the Hedgehog pathway (Figures 3a-c). To explore the regulatory role of HIF-1 α , Vector, HIF-1 α , sh-NC, and sh-HIF-1 α constructs were transfused into SK-OV-3 OCSCs. HIF-1 α expression increased by 1.72-fold after HIF-1 α overexpression, whereas sh-HIF-1 α transfection reduced expression by 52% ($p < 0.001$; Figures 3d, e), confirming successful generation of HIF-1 α overexpression and knockdown cell lines. In cells with HIF-1 α overexpression, levels of p-PI3K (2.22-fold), p-AKT (1.68-fold), Smo (1.58-fold), SHH (1.55-fold), and Gli1 (1.48-fold) protein levels were significantly upregulated. Conversely, HIF-1 α knockdown reduced p-PI3K (-41%), p-AKT (-51%), Smo (-35%), SHH (-44%), and Gli1 (-68%) protein levels (all $p < 0.001$; Figures 3d-f). Furthermore, when transfected cells were cultured under hypoxia for 24 h, HIF-1 α overexpression further increased HIF-1 α levels and enhanced PI3K and Hedgehog pathway activation. In contrast, HIF-1 α knockdown decreased HIF-1 α expression and significantly suppressed activation of both pathways ($p < 0.001$; Figures 3g-i). Collectively, these findings indicate that HIF-1 α regulates PI3K and Hedgehog signaling, both of which are closely associated with VM formation in SK-OV-3 OCSCs.

Knockdown of HIF-1 α inhibited the EET of OCSCs induced by hypoxia and suppressed VM formation through the PI3K and Hedgehog signaling pathways

To verify whether HIF-1 α regulates VM in OCSCs via the PI3K and Hedgehog signaling pathways, SK-OV-3 OCSCs with HIF-1 α knockdown were treated with the PI3K agonist 740 Y-P, PI3K inhibitor LY294002, Hedgehog agonist purmorphamine, or Hedgehog inhibitor cyclopamine, followed by 24 h of hypoxia. Compared with the hypoxia + sh-HIF-1 α group, 740 Y-P and LY294002 did not affect HIF-1 α levels; however, 740 Y-P significantly increased p-PI3K (+56%) and p-AKT (+24%) expressions, while LY294002 decreased p-PI3K (-23%) and p-AKT (-20%) expressions ($p < 0.001$; Figure 4a). Similarly, purmorphamine upregulated Smo (+36%), SHH (+27%), and Gli1 (+21%) protein levels, whereas cyclopamine suppressed Smo (-28%), SHH (-22%), and Gli1 (-23%) expression ($p < 0.001$; Figure 4b). Hypoxia was also observed to induce epithelium-to-endothelium transition (EET) of CSCs during VM formation.⁹ After hypoxia, E-cadherin (epithelial marker) expression decreased by 46%, while N-cadherin (+2.05-fold) and VE-cadherin (+2.09-fold) (endothelial markers) were upregulated. In contrast, HIF-1 α knockdown reversed this trend, increasing E-cadherin (+56%) and reducing N-cadherin (-25%) and VE-cadherin (-28%) levels ($p < 0.001$; Figure 4c). These findings indicate that HIF-1 α knockdown inhibits hypoxia-induced

EET and consequently suppresses VM formation through modulation of the PI3K and Hedgehog pathways. The 3D culture experiments demonstrated that SK-OV-3 OCSCs elongated into spindle-like shapes within the Matrigel matrix, forming protrusions that interconnected to create crisscrossing tubular structures and grid-like networks. Under hypoxic conditions, the number of branching points ($46.91 \rightarrow 89.35$) and 3D channels ($134.86 \rightarrow 170.35$) significantly increased ($p < 0.001$), accompanied by enhanced intercellular connections that maintained a stable grid-like structure. In contrast, HIF-1 α knockdown markedly reduced branching points ($86.31 \rightarrow 56.35$) and 3D channels ($174.54 \rightarrow 139.26$) ($p < 0.001$). Cells exhibited fewer protrusions, slower and irregular intercellular connections, and diminished grid formation (Figures 4d-f), indicating that HIF-1 α knockdown inhibited hypoxia-induced VM formation. Moreover, 740 Y-P and purmorphamine attenuated the inhibitory effects of HIF-1 α knockdown on EET and VM formation, whereas LY294002 and cyclopamine enhanced these inhibitory effects (Figures 4c-f). Collectively, these results demonstrate that HIF-1 α knockdown suppresses the PI3K and Hedgehog signaling pathways, thereby blocking hypoxia-induced EET and VM formation in SK-OV-3 OCSCs.

Knockdown of HIF-1 α inhibited the growth and invasion of OCSCs in a hypoxic environment through the PI3K and Hedgehog signaling pathways

Because VM is a tumor angiogenesis pattern dependent on tumor cells, it promotes CSC growth.¹¹ Consistently, this study found

that the viability (Figure 5a) and proportion of EdU-positive cells (Figure 5b) of SK-OV-3 OCSCs significantly increased under hypoxic conditions but markedly decreased after HIF-1 α knockdown ($p < 0.001$). The number of invasive cells also rose ($50.12 \rightarrow 96.33$) in response to hypoxia but fell ($94.33 \rightarrow 65.67$) after HIF-1 α knockdown ($p < 0.001$; Figure 5c), indicating that HIF-1 α knockdown suppressed OCSC proliferation and invasion in hypoxic environments. Western blot analysis supported these findings: hypoxia markedly elevated the protein expression of Ki-67, MMP2, and MMP9 (2.13-, 2.02-, and 2.10-fold, respectively), whereas HIF-1 α knockdown reduced their expression by 29%, 28%, and 26% ($p < 0.001$; Figure 5d). Furthermore, relative to the hypoxia + sh-HIF-1 α group, proliferation and invasion capacities were significantly enhanced following 740 Y-P and purmorphamine treatment but were further suppressed by LY294002 and cyclopamine (Figures 5a-d). These findings suggest that HIF-1 α knockdown inhibits the proliferation and invasion of SK-OV-3 OCSCs by downregulating the PI3K and Hedgehog signaling pathways.

Inhibition of the PI3K and Hedgehog signaling pathways suppressed VM formation in xenografted OCSCs

CSCs isolated from the SK-OV-3 cell line were implanted into the brains of Nu/Nu mice, which subsequently received intraperitoneal injections of 740 Y-P, LY294002, purmorphamine, or cyclopamine twice weekly for 4 weeks. Tumor volume was measured weekly. Treatment with 740 Y-P and purmorphamine significantly increased

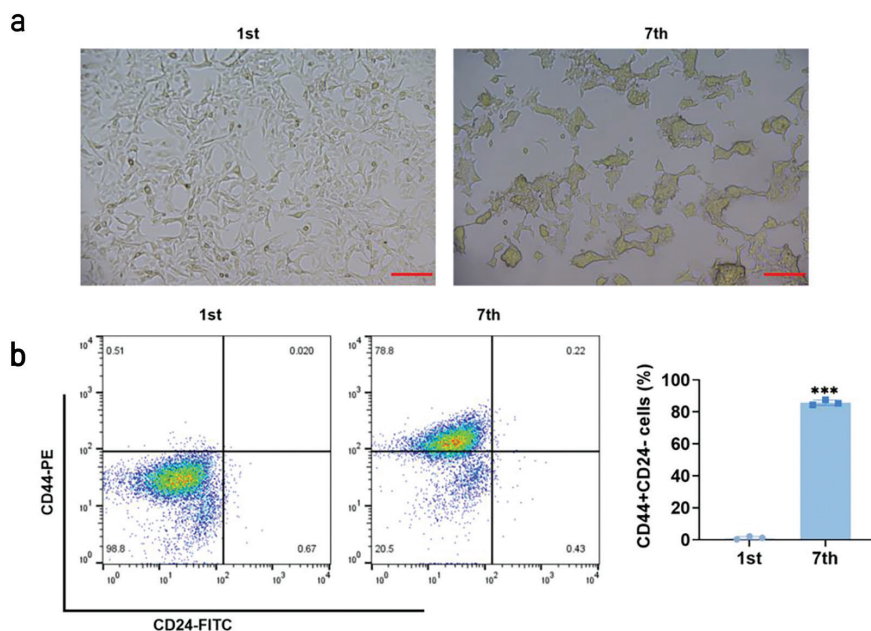


FIG. 1. Identification of OCSCs.

(a) SK-OV-3 cells were cultured in serum-free medium, and the morphology of the first and seventh generations was recorded. With the passage of cells, the number of suspended sphere cells increased and the volume increased ($\times 10, 200 \mu\text{m}$). (b) Flow cytometry assay for CD44 + CD24- phenotype cells. The number of CD44 + CD24- phenotype cells in the seventh generation SK-OV-3 cells accounted for the majority. $n = 3$, data are represented as mean \pm SD, *** $p < 0.001$ vs. 1st group. The comparison between two independent cohorts used the Student's t-test. OCSCs, ovarian cancer stem cells; SD, standard deviation.

SD, standard deviation; OCSCs, ovarian cancer stem cells.

tumor volume ($p = 0.043$; $188.8 \text{ mm}^3 \rightarrow 386.4 \text{ mm}^3$ and $188.8 \text{ mm}^3 \rightarrow 377.0 \text{ mm}^3$, respectively) and weight ($p < 0.001$; $198.24 \text{ mg} \rightarrow 405.72 \text{ mg}$ and $198.24 \text{ mg} \rightarrow 395.85 \text{ mg}$, respectively). In contrast, LY294002 and cyclopamine significantly reduced tumor volume ($p = 0.036$; $188.8 \text{ mm}^3 \rightarrow 102.1 \text{ mm}^3$ and $188.8 \text{ mm}^3 \rightarrow 116.0 \text{ mm}^3$, respectively) and weight ($p < 0.001$; $198.24 \text{ mg} \rightarrow 107.10 \text{ mg}$ and $198.24 \text{ mg} \rightarrow 121.82 \text{ mg}$, respectively) (Figures 6a-c).

Immunohistochemistry revealed that Ki-67-positive cells increased after 740 Y-P and purmorphamine treatment but decreased significantly after LY294002 and cyclopamine intervention (Figure 6d), indicating that PI3K and Hedgehog inhibition suppressed OCSC growth. PAS staining showed a similar pattern: PAS-positive cells were elevated with 740 Y-P and purmorphamine but reduced with LY294002 and cyclopamine ($p < 0.001$, Figures 6e, f). Consistently, the number of CD31-positive cells, marking angiogenesis, followed the same trend as PAS staining (Figure 6d). This indicated that 740 Y-P and purmorphamine promoted VM formation, whereas LY294002 and cyclopamine inhibited VM formation. Western blot analysis further showed that p-PI3K and p-AKT protein levels increased 1.38- and 1.94-fold, respectively, after 740 Y-P treatment but decreased by 72% and 41%, respectively, after LY294002

treatment ($p < 0.001$, Figure 6g). Similarly, the expression of Smo, SHH, and Gli1 proteins increased 1.51-, 1.94-, and 1.89-fold, respectively, after purmorphamine treatment but decreased by 38%, 25%, and 40%, respectively, after cyclopamine treatment ($p < 0.001$, Figure 6h). Following 740 Y-P and purmorphamine treatment, E-cadherin protein levels were significantly reduced (-49% and -34%, respectively; $p < 0.001$ and $p = 0.007$), whereas N-cadherin (2.08- and 1.45-fold; $p < 0.001$, $p = 0.019$, $p = 0.004$), VE-cadherin (1.83- and 1.50-fold; $p < 0.001$ and $p = 0.006$), MMP2 (1.55- and 1.53-fold; $p < 0.001$), and MMP9 (1.71- and 1.57-fold; $p < 0.001$) were significantly upregulated. In contrast, these protein expression changes were reversed after LY294002 and cyclopamine treatment (Figures 6i-k). In summary, inhibition of the PI3K and Hedgehog signaling pathways suppressed both growth and VM formation of xenografted OCSCs.

DISCUSSION

OCSCs are known to increase the risk of invasion and metastasis and are a major cause of tumor recurrence and chemotherapy resistance.⁶ Consequently, elucidating the mechanisms underlying OCSC function and identifying novel therapeutic targets has

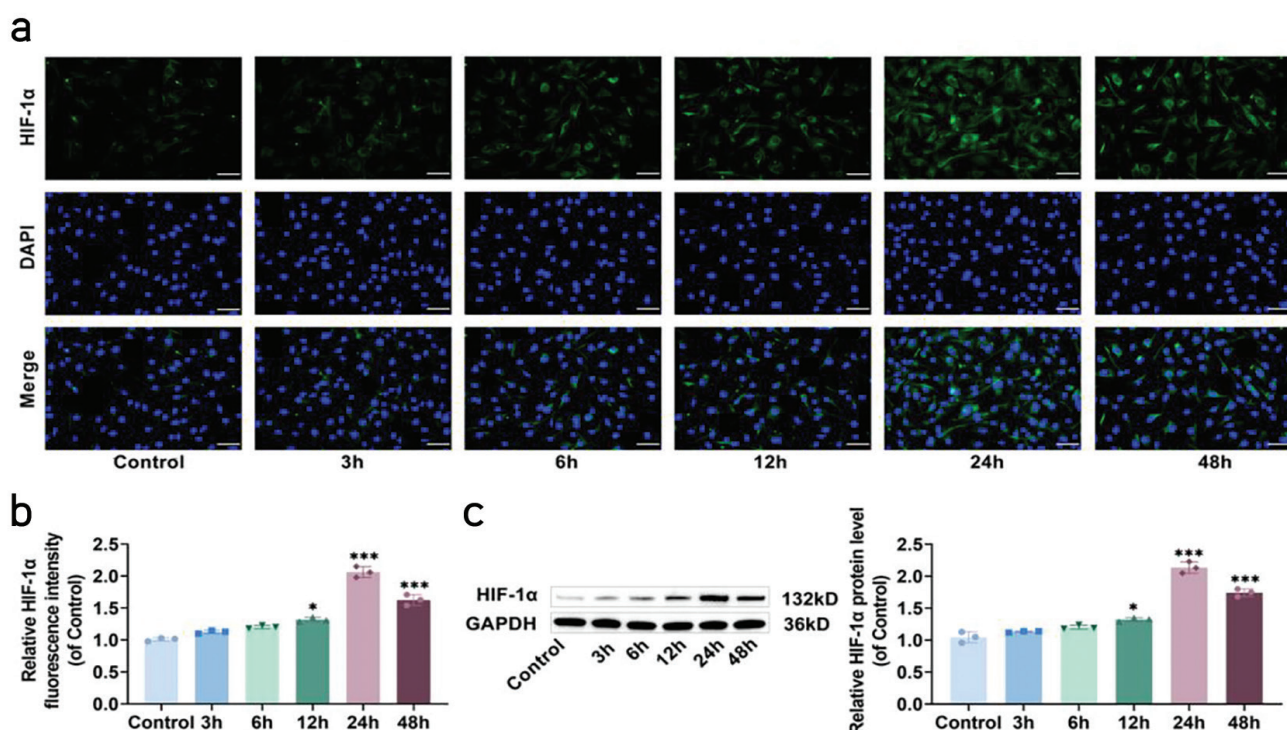


FIG. 2. Hypoxia could induce HIF-1 α level of SK-OV-3 OCSCs.

(a, b) SK-OV-3 OCSCs were treated with CoCl₂ for 0, 3, 6, 12, 24 and 48 h, and HIF-1 α expressions were discovered through immunofluorescence. The fluorescence intensity of HIF-1 α was significantly increased after hypoxia for 12 h ($\times 40$, 50 μm). (c) HIF-1 α protein was discovered by Western blot. It was significantly increased at 24 and 48 h of hypoxia.

n = 3, data are represented as mean \pm SD, * $p < 0.05$, *** $p < 0.001$ vs. control group. One-way ANOVA followed by Tukey's honest significant difference as a post-hoc test to determine the corrected significance of comparison between multiple groups, or Kruskal-Wallis test followed by Dunn's test as a post-hoc test to ascertain the corrected significance of comparison between multiple groups was used where appropriate.

OCSCs, ovarian cancer stem cells; HIF-1 α , hypoxia-inducible factor-1 α ; SD, standard deviation.

become a research focus in the clinical treatment of OC. VM has been reported not only in OC but also in renal cell carcinoma, liver cancer, gallbladder cancer, nasopharyngeal carcinoma, and other malignancies.^{21,23-26} VM is closely associated with tumor invasion and metastasis, providing nutritional support that sustains tumor growth

and dissemination. CD44⁺/CD24⁻ is one of the most well-established surface markers of CSCs.^{19,20} In this study, SK-OV-3 cells were sorted using a serum-free suspension culture method, and their biological characteristics were assessed. Cells with CSC-like properties were successfully isolated and referred to as OCSCs, enabling exploration

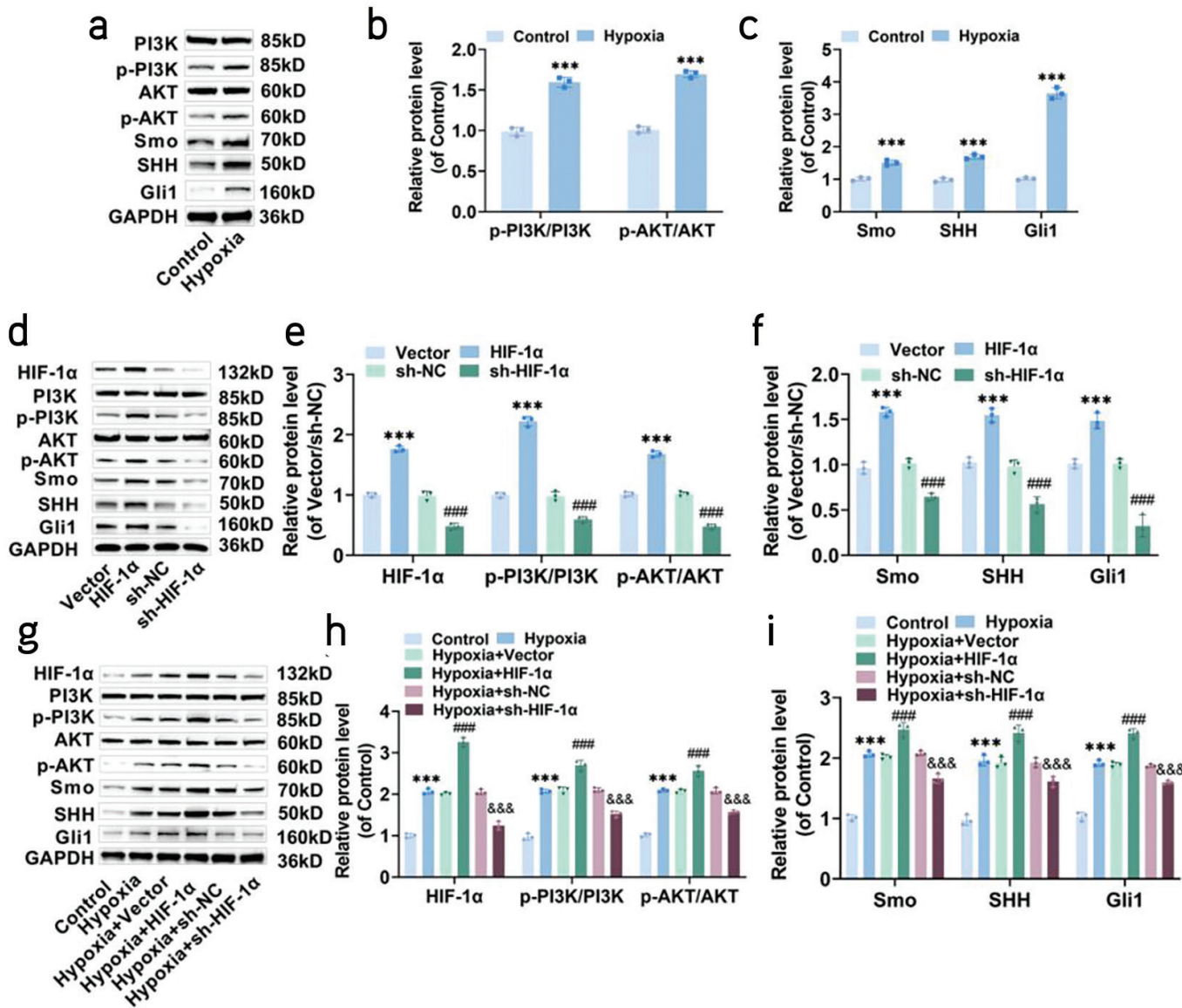


FIG. 3. Knockdown of HIF-1 α expression suppressed PI3K signaling pathway and Hedgehog signaling pathway activation in hypoxic environment. (a-c) PI3K signaling pathway and Hedgehog signaling pathway proteins were detected by Western blot. p-PI3K, p-AKT, Smo, SHH and Gli1 expressions were significantly increased after hypoxia. (d-f) Vector, HIF-1 α , sh-NC and sh-HIF-1 α plasmids were transfected into SK-OV-3 OCSCs, and the expressions of PI3K signaling pathway and Hedgehog pathway increased after HIF-1 α overexpression and decreased after HIF-1 α knockdown. (g-i) The transfected SK-OV-3 OCSCs were placed in a hypoxic environment for 24 h, and the expressions of PI3K and Hedgehog pathway were detected through Western blot. Under hypoxic conditions, p-PI3K, p-AKT, Smo, SHH and Gli1 proteins increased after HIF-1 α overexpression and decreased after HIF-1 α knockdown.

n = 3, data are represented as mean \pm SD, ***p < 0.001 vs. control or Vector group; ###p < 0.001 vs. sh-NC or Hypoxia + Vector group; &&p < 0.001 vs. Hypoxia + sh-NC group. One-way ANOVA followed by Tukey's honest significant difference as a post-hoc test to determine the corrected significance of comparison between multiple groups, or Kruskal-Wallis test followed by Dunn's test as a post-hoc test to ascertain the corrected significance of comparison between multiple groups was used where appropriate.

OCSCs, ovarian cancer stem cells; HIF-1 α , hypoxia-inducible factor-1 α ; PI3K, phosphatidylinositol 3-kinase; AKT, protein kinase B; Smo, smoothened; SHH, sonic hedgehog; SD, standard deviation.

of their relationship with VM formation and its potential molecular mechanisms.

Serum-free suspension culture is a widely used method for enriching tumor stem cells.²⁷ In the present experiment, a subset of suspended

cells demonstrated robust growth upon subculture, displaying self-renewal and continuous proliferation. Flow cytometry revealed that CD44⁺/CD24⁻ cells accounted for only a small proportion of the first-generation SK-OV-3 cells, but their proportion increased dramatically to 85.76 ± 1.64% in the seventh generation.

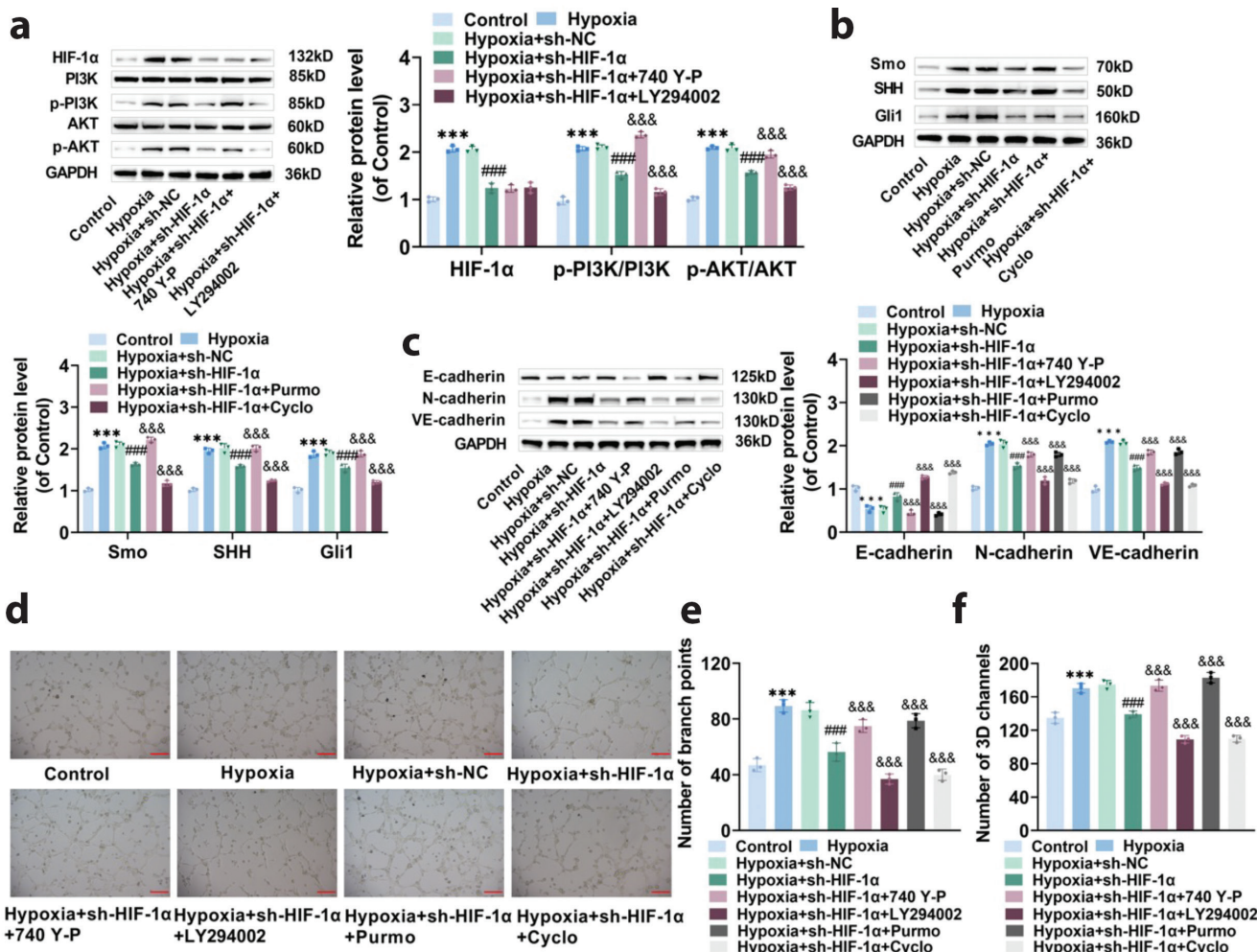


FIG. 4. Knockdown of HIF-1 α inhibited the EET of OCSCs induced through hypoxia and inhibited VM formation through PI3K and Hedgehog signaling pathway.

(a) 740 Y-P and LY294002 were added to the transfected SK-OV-3 OCSCs, and then they were placed in an hypoxic environment. PI3K pathway protein expressions were detected using Western blot. 740 Y-P increased p-PI3K and p-AKT expressions after 740 Y-P intervention, and decreased after LY294002 treatment. (b) The transfected SK-OV-3 OCSCs were added with 740 Y-P and LY294002, and then placed in an hypoxic environment. Hedgehog pathway proteins were detected using Western blot. Smo, SHH and Gli1 expressions increased after Purmorphamine intervention and decreased after Cyclopamine treatment. (c) E-cadherin, N-cadherin and VE-cadherin protein expressions were detected by Western blot. After hypoxia, E-cadherin expression lessened, N-cadherin and VE-cadherin expressions elevated. After HIF-1 α knockdown, the protein levels were significantly reversed. (d-f) VM ability was detected by matrigel 3D culture experiment. The number of branching points and 3D channels increased significantly under hypoxic conditions, and decreased significantly after HIF-1 α knockdown ($\times 10$, 200 μ m).

n = 3, data are represented as mean \pm SD, ***p < 0.001 vs. control group; #p < 0.001 vs. Hypoxia + sh-NC group; &&p < 0.001 vs. Hypoxia + sh-HIF-1 α group. One-way ANOVA followed by Tukey's honest significant difference as a post-hoc test to determine the corrected significance of comparison between multiple groups, or Kruskal-Wallis test followed by Dunn's test as a post-hoc test to ascertain the corrected significance of comparison between multiple groups was used where appropriate.

OCSCs, ovarian cancer stem cells; HIF-1 α , hypoxia-inducible factor-1 α ; EET, epithelium-to-endothelium transition; VM, vasculogenic mimicry; PI3K, phosphatidylinositol 3-kinase; AKT, protein kinase B; Smo, smoothened; SHH, sonic hedgehog; SD, standard deviation.

These findings confirm that serum-free suspension culture can be used to enrich and purify OC cells with CSC-like properties, thereby successfully inducing OCSCs.

Unlike traditional tumor angiogenesis, VM is composed of tumor cells that form tubular structures to transport nutrients and oxygen, thereby sustaining tumor growth and driving malignant progression.²⁸ Hypoxia is a hallmark of the tumor microenvironment

and a key inducer of malignant transformation. It triggers numerous adaptive changes in tumor cells, and accumulating evidence indicates that hypoxia is closely linked to VM development.⁹ HIF-1 α is tightly regulated by cellular oxygen content and functions as a sensor of extracellular oxygen concentration. The rapid growth of malignant tumors frequently results in localized hypoxia; in this context, HIF-1 α acts as a crucial mediator of cellular adaptation and serves as an internal marker of hypoxia.²⁹

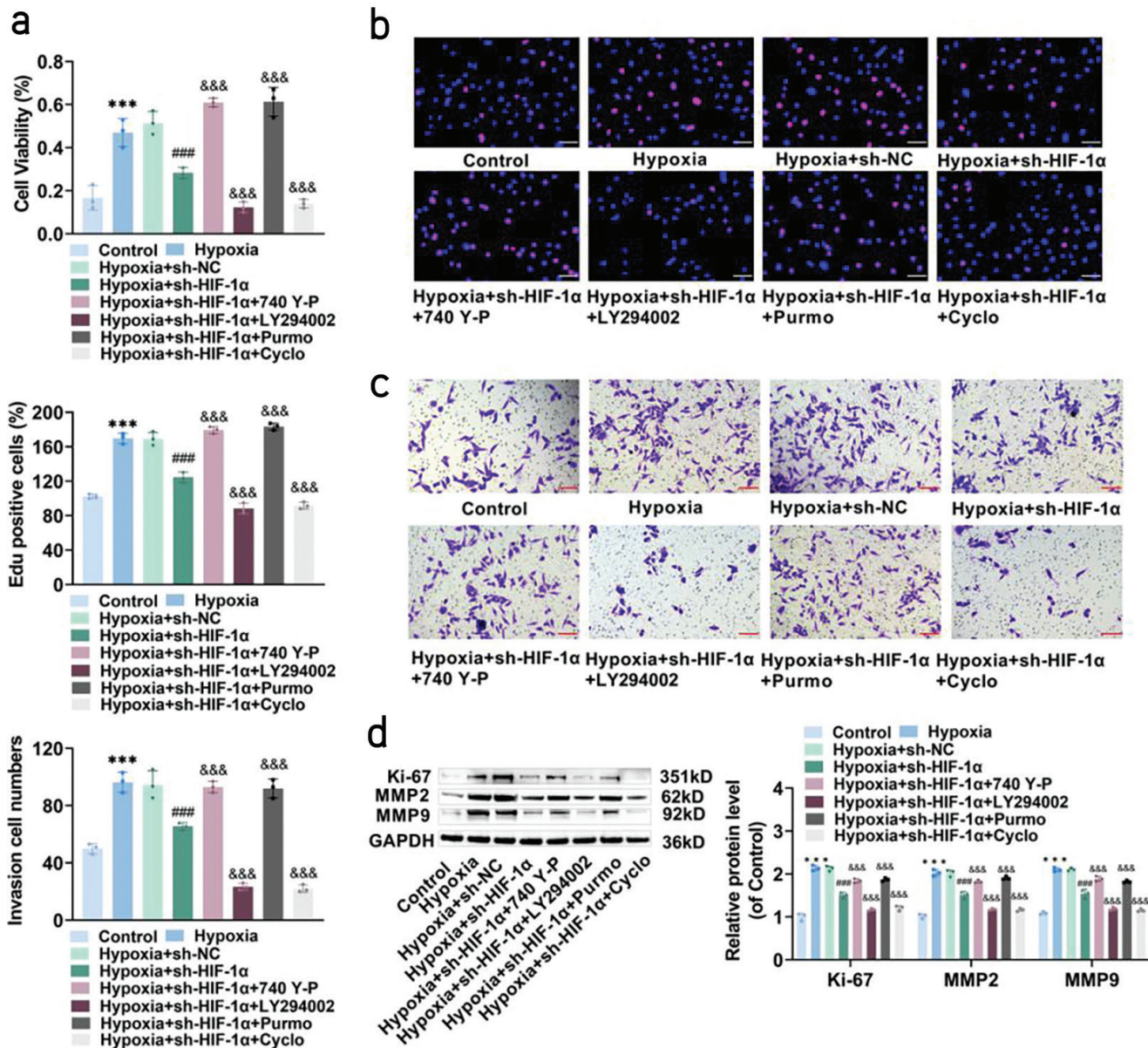
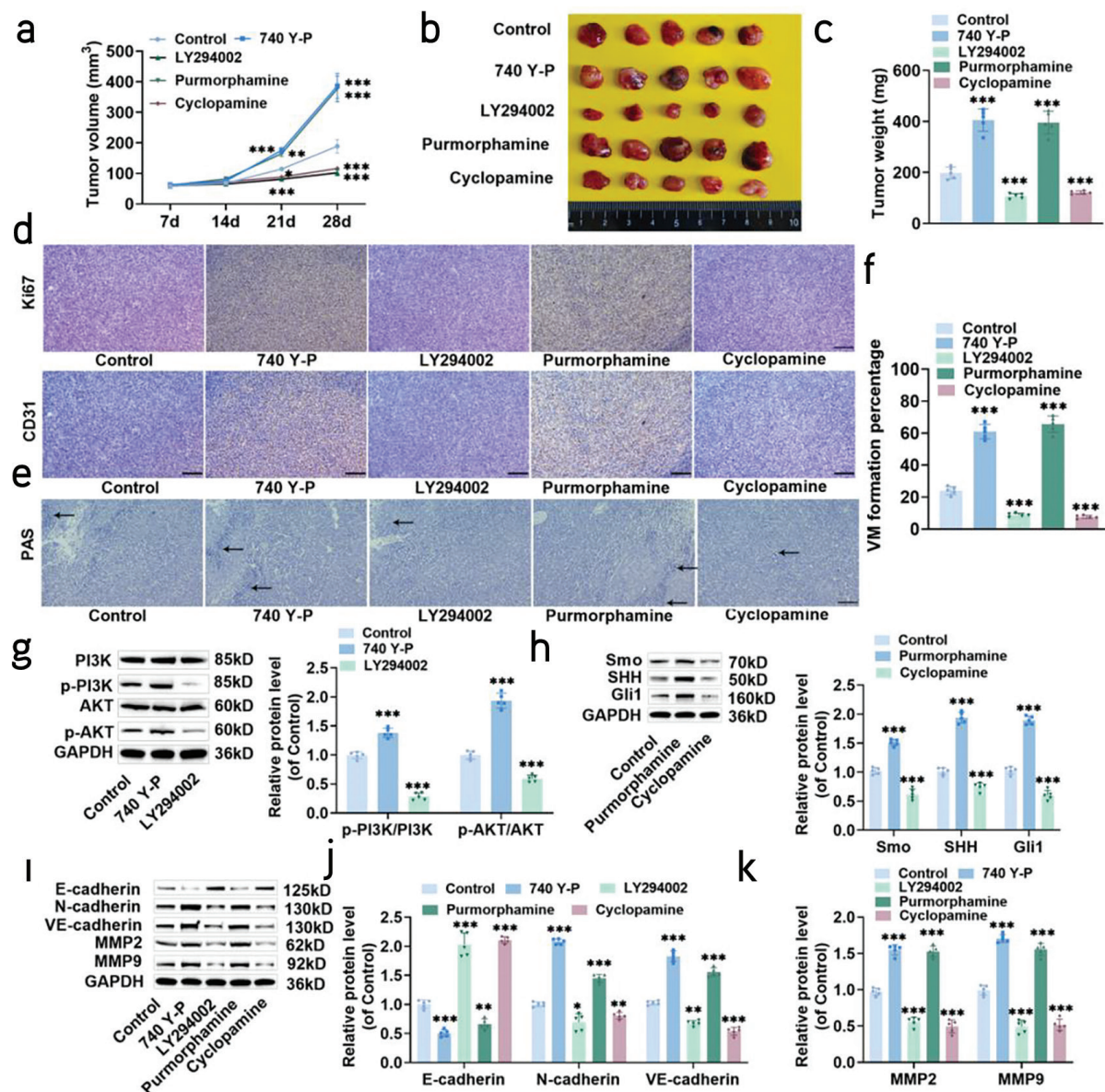


FIG. 5. Knockdown of HIF-1 α inhibited the proliferation and invasion of OCSCs in hypoxic environment through PI3K and Hedgehog signaling pathway. (a) Cell viability was detected by MTS experiment. It was significantly increased in hypoxic environment or after 740 Y-P and Purmorphamine intervention, and significantly decreased after HIF-1 α knockdown or LY294002 and Cyclopamine intervention. (b) Cell proliferation was detected by EdU experiment. EdU positive cells increased significantly in hypoxic environment or after 740 Y-P and Purmorphamine intervention, and decreased significantly after HIF-1 α knockdown or LY294002 and Cyclopamine intervention ($\times 40, 50 \mu\text{m}$). (c) Cell invasion was detected by Transwell experiment. The number of invasive cells increased significantly in hypoxic environment or after 740 Y-P and Purmorphamine intervention, and decreased significantly after HIF-1 α knockdown or LY294002 and Cyclopamine intervention ($\times 20, 100 \mu\text{m}$). (d) Ki-67, MMP2 and MMP9 expressions.

**FIG. 6. In vivo experiment.**

(a-c) OCSCs were implanted into the intracranial cavity of mice, and 740 Y-P, LY294002, Purmorphamine and Cyclopamine were injected intraperitoneally twice a week. The tumor volume was monitored weekly, and the tumor was stripped and weighed after 4 weeks. Tumor volume and weight increased significantly after 740 Y-P and Purmorphamine intervention, and decreased significantly after LY294002 and Cyclopamine intervention. (d) Ki-67 and CD31 expressions in tumor tissues were detected by immunohistochemistry. They increased significantly after 740 Y-P and Purmorphamine intervention, and decreased significantly after LY294002 and Cyclopamine intervention ($\times 20, 100 \mu\text{m}$). (e, f) PAS staining was used to detect angiogenesis in tumor tissues. 740 Y-P and Purmorphamine could promote VM formation, while LY294002 and Cyclopamine could inhibit VM formation ($\times 20, 100 \mu\text{m}$). (g) PI3K pathway protein expressions were detected by Western blot. The expression of p-PI3K and p-AKT increased notably when 740 Y-P intervention, and decreased significantly after LY294002 intervention. (h) Hedgehog pathway protein expressions were detected by Western blot. The expression of Smo, SHH and Gli1 protein increased significantly after Purmorphamine intervention, and decreased significantly after Cyclopamine intervention. (i-k) VM formation and invasion-related protein levels in tumor tissues were detected by Western blot. When 740 Y-P and Purmorphamine treatment, E-cadherin level was significantly decreased, N-cadherin, VE-cadherin, MMP2 and MMP9 protein expressions were significantly increased. However, after LY294002 and Cyclopamine treatment, the above protein levels were significantly reversed.

$n = 5$, data are represented as mean \pm SD, * $p < 0.05$, ** $p < 0.01$, *** $p < 0.001$ vs. control group. Repeated-measures ANOVA was used to analyze the tumor growth curve. One-way ANOVA followed by Tukey's Honest Significant Difference as a post-hoc test to determine the corrected significance of comparison between multiple groups, or Kruskal-Wallis test followed by Dunn's test as a post-hoc test to ascertain the corrected significance of comparison between multiple groups was used where appropriate.

OCSCs, ovarian cancer stem cells; HIF-1 α , hypoxia-inducible factor-1 α ; PI3K, phosphatidylinositol 3-kinase; PI3K, phosphatidylinositol 3-kinase; AKT, protein kinase B; Smo, smoothened; SHH, sonic hedgehog; MMP, matrix metalloproteinase; SD, standard deviation.

Previous studies have shown that hypoxic conditions upregulate HIF-1 α expression in tumor cells and promote VM formation³⁰, whereas HIF-1 α downregulation suppresses VM-like structure formation and inhibits glioma growth.³¹ In this study, the expression of HIF-1 α in SK-OV-3 OCSCs was markedly increased under CoCl₂-induced hypoxic conditions. This may reflect the rapid proliferation of OCSCs, which creates an insufficient endothelial-dependent blood supply. To adapt to this ischemic and hypoxic state, tumor cells increase HIF-1 α expression, activate downstream target genes, and ultimately promote VM formation.

Previous studies have shown that HIF-1 α expression is regulated by the PI3K/AKT pathway, and inactivation of this pathway results in reduced HIF-1 α expression.^{32,33} Other evidence suggests that HIF-1 α may act as an inducer of Hedgehog signaling. Wei et al.³⁴ reported that HIF-1 α promotes autocrine secretion of SHH in glioma cells, thereby activating the Hedgehog pathway, whereas the HIF-1 α inhibitor AMSP-30m suppresses Hedgehog pathway activity.³⁵ The PI3K/AKT pathway is initiated when PI3K activates AKT through phosphatidylinositol family members and plays a critical role in OC progression, including growth, metastasis, drug resistance, and angiogenesis.^{36,37} Hedgehog signaling consisted of four major components: ligands (SHH, IHH, and DHH), transmembrane receptors (Ptch and Smo), nuclear transcription factors (Gli1, Gli2, and Gli3), and downstream target genes.³⁸ SHH is essential for gonadal tissue growth and function³⁹, including ovarian and follicular development. Smo is a seven-transmembrane receptor protein⁴⁰ whose cysteine-rich domain is required for Hedgehog activity, while Gli1 primarily functions as transcriptional activator. Activation of Hedgehog signaling has been shown to promote tumor VM.¹⁸ Furthermore, inhibition of both Hedgehog and PI3K pathways suppresses tumor growth, stem cell-like properties, and stem cell marker expression.⁴¹ Conversely, activation of Hedgehog and PI3K/AKT signaling enhances the multidirectional differentiation potential of CSCs in various cancers^{9,42}, whereas inhibition of these pathways reduces cancer cell proliferation and endothelial cell angiogenesis.^{36,43-46}

The results of this study showed that the levels of p-PI3K, p-AKT, Smo, SHH, and Gli1 proteins were significantly increased after 24 h of hypoxia in SK-OV-3 OCSCs, indicating activation of the PI3K/AKT and Hedgehog signaling pathways. In contrast, HIF-1 α knockdown inhibited the activation of both pathways. These findings suggest that PI3K/AKT and Hedgehog signaling are involved in the VM-forming capacity of SK-OV-3 OCSCs.

Three key factors contribute to hypoxia-induced VM formation: CSCs, EET, and tumor extracellular matrix (ECM) remodeling. During EET, tumor stem cells lose epithelial markers and acquire endothelial-like properties, forming VM structures on the remodeled ECM "scaffold". E-cadherin, an epithelial marker responsible for maintaining tight junctions between cells, decreases during this process. Reduced E-cadherin expression weakens intercellular adhesion, causing cancer cells to lose polarity and connectivity, thereby gaining motility and invasive potential.⁴⁷ N-cadherin, a single-chain transmembrane glycoprotein, mediates adhesion between different cell types and plays important roles in tumor transformation, apoptosis, and angiogenesis.⁴⁸ VE-cadherin, which

mediates adhesion between adjacent endothelial cells, is critical for vascular integrity and regulation of endothelial permeability. Experimental evidence shows that VE-cadherin promotes adhesion of mouse breast cancer cells to VE cells *in vitro*, facilitating tumor dissemination and metastasis.⁴⁹ Another study reported that phosphorylation of VE-cadherin reduced VM formation in human breast cancer.⁵⁰ Collectively, these findings highlight the central role of VE-cadherin in VM development.

Currently, 3D culture is an important *in vitro* model for studying VM, as it more closely mimics the *in vivo* growth environment. Under hypoxic conditions, E-cadherin expression decreased, whereas N-cadherin and VE-cadherin expressions increased in OCSCs. Hypoxia also promoted earlier formation of VM tubular structures in SK-OV-3 OCSCs, with a more regular grid pattern, increased numbers of branch points and 3D channels, and greater structural plasticity, indicating that hypoxia induced EET and VM formation. In addition, the proliferative and invasive capacities of SK-OV-3 OCSCs were significantly enhanced by hypoxia. Knockdown of HIF-1 α suppressed EET, VM formation, and the proliferation and invasion of OCSCs. Importantly, treatment with 740 Y-P and purmorphamine attenuated the inhibitory effects of HIF-1 α knockdown, whereas LY294002 and cyclopamine enhanced them. These findings suggest that HIF-1 α knockdown inhibits activation of the PI3K and Hedgehog pathways, thereby blocking EET, VM formation, and the malignant phenotype of SK-OV-3 OCSCs.

Finally, OCSCs were implanted into the brains of Nu/Nu mice, and 740 Y-P, LY294002, purmorphamine, and cyclopamine were administered intraperitoneally. Treatment with 740 Y-P and purmorphamine significantly promoted OCSC growth, proliferation, EET, and VM formation, accompanied by activation of the PI3K and Hedgehog pathways. In contrast, LY294002 and cyclopamine exerted the opposite effects, suppressing these processes. These results indicate that inhibition of PI3K and the Hedgehog signaling suppresses VM formation in xenografted OCSCs. Thus, both pathways play critical roles in OC progression by promoting VM formation, and they may regulate CSC properties and EET in OC.

In summary, this study successfully induced the formation of OCSC and demonstrated that inhibition of the PI3K and Hedgehog signaling pathways significantly reduced hypoxia-induced OCSC proliferation, EET, and VM formation. These findings provide theoretical support for the development of new anti-vascular therapeutic strategies in OC and suggest novel avenues for targeted therapy. However, this study has limitations. Further *in vivo* and clinical investigations are needed to clarify whether inhibition of these pathways suppresses VM formation through OCSCs. Moreover, given the complexity of VM formation, the precise molecular mechanisms by which the PI3K and Hedgehog pathways regulate this process warrant further exploration.

Ethics Committee Approval: All animal experiments were approved by the Ethics Committee of the Third Hospital of Hebei Medical University (approval number: 2025-083-1, date: 12.06. 2025).

Informed Consent: Not available.

Data Sharing Statement: The datasets analyzed during the current study are available from the corresponding author upon reasonable request.

Authorship Contributions: Supervision- H.Z.; Writing- J.L.; Critical Review- Y.B.

Conflict of Interest: The authors declare that they have no conflict of interest.

Funding: The authors declared that this study received no financial support.

REFERENCES

- Vajjihe H, Leila S, Sadri F. Exploring ferroptosis and epigenetic regulation in Gynecological Cancers: Implications for Treatment Strategies. *Journal of Cancer Biomolecules and Therapeutics*. 2025;2:37-54. [\[CrossRef\]](#)
- Sung H, Ferlay J, Siegel RL, et al. Global Cancer Statistics 2020: GLOBOCAN estimates of incidence and mortality worldwide for 36 cancers in 185 countries. *CA Cancer J Clin*. 2021;71:209-249. [\[CrossRef\]](#)
- Liang X, Yu C, Tian Y, Xiang X, Luo Y. Inhibition of STX17-SNAP29-VAMP8 complex formation by costunolide sensitizes ovarian cancer cells to cisplatin via the AMPK/mTOR signaling pathway. *Biochem Pharmacol*. 2023;212:115549. [\[CrossRef\]](#)
- Armstrong DK, Alvarez RD, Backes FJ, et al. NCCN Guidelines® Insights: Ovarian Cancer, Version 3.2022. *J Natl Compr Canc Netw*. 2022;20:972-80. [\[CrossRef\]](#)
- Ahmed N, Kadife E, Raza A, Short M, Jubinsky PT, Kouroukakis G. Ovarian cancer, cancer stem cells and current treatment strategies: a potential role of magmas in the current treatment methods. *Cells*. 2020;9:719. [\[CrossRef\]](#)
- Muñoz-Galván S, Carnero A. Targeting cancer stem cells to overcome therapy resistance in ovarian cancer. *Cells*. 2020;9:1402. [\[CrossRef\]](#)
- Battistini C, Kenny HA, Zambuto M, et al. Tumor microenvironment-induced FOXM1 regulates ovarian cancer stemness. *Cell Death Dis*. 2024;15:370. [\[CrossRef\]](#)
- Huang Z, Byrd O, Tan S, et al. Periostin facilitates ovarian cancer recurrence by enhancing cancer stemness. *Sci Rep*. 2023;13:21382. [\[CrossRef\]](#)
- Wei X, Chen Y, Jiang X, et al. Mechanisms of vasculogenic mimicry in hypoxic tumor microenvironments. *Mol Cancer*. 2021;20:7. [\[CrossRef\]](#)
- Tian X, Si Q, Liu M, et al. Advance in vasculogenic mimicry in ovarian cancer (Review). *Oncol Lett*. 2023;26:456. [\[CrossRef\]](#)
- Luo Q, Wang J, Zhao W, et al. Vasculogenic mimicry in carcinogenesis and clinical applications. *J Hematol Oncol*. 2020;13:19. [\[CrossRef\]](#)
- Liu J, Zhang J, Zhang Y, Yang B, Liu H, Chen Y. MATN2 overexpression suppresses tumor growth in ovarian cancer via PTEN/PI3K/AKT pathway. *Funct Integr Genomics*. 2024;24:71. [\[CrossRef\]](#)
- Wang Y, Luo X, Wu N, Liao Q, Wang J. SRC-3/TRAF4 facilitates ovarian cancer development by activating the PI3K/AKT signaling pathway. *Med Oncol*. 2023;40:76. [\[CrossRef\]](#)
- Jin L, Chen C, Huang L, Bu L, Zhang L, Yang Q. Salvianolic acid A blocks vasculogenic mimicry formation in human non-small cell lung cancer via PI3K/Akt/mTOR signalling. *Clin Exp Pharmacol Physiol*. 2021;48:508-514. [\[CrossRef\]](#)
- Liu H, Zhang J, Zhao Y, et al. CD93 regulates breast cancer growth and vasculogenic mimicry through the PI3K/AKT/SP2 signaling pathway activated by integrin β1. *J Biochem Mol Toxicol*. 2024;38:23688. [\[CrossRef\]](#)
- Huang J, Wang C, Hou Y, et al. Molecular mechanisms of Thrombospondin-2 modulates tumor vasculogenic mimicry by PI3K/AKT/mTOR signaling pathway. *Biomed Pharmacother*. 2023;167:115455. [\[CrossRef\]](#)
- Karin-Kujundzic V, Covarrubias-Pinto A, Skrtic A, Vranic S, Serman L. New insight into the role of PTCH1 protein in serous ovarian carcinomas. *Int J Oncol*. 2022;61:145. [\[CrossRef\]](#)
- You X, Wu J, Wang Y, et al. Galectin-1 promotes vasculogenic mimicry in gastric adenocarcinoma via the Hedgehog/GLI signaling pathway. *Aging (Albany NY)*. 2020;12:21837-21853. [\[CrossRef\]](#)
- Resendiz-Hernández M, García-Hernández AP, Silva-Cázares MB, et al. MicroRNA-204 regulates angiogenesis and vasculogenic mimicry in CD44+/CD24- breast cancer stem-like cells. *Noncoding RNA*. 2024;10:14. [\[CrossRef\]](#)
- Maroufi NF, Amiri M, Dizaji BF, et al. Inhibitory effect of melatonin on hypoxia-induced vasculogenic mimicry via suppressing epithelial-mesenchymal transition (EMT) in breast cancer stem cells. *Eur J Pharmacol*. 2020;881:173282. [\[CrossRef\]](#)
- Recouvreux MS, Miao J, Gozo MC, et al. FOXC2 promotes vasculogenic mimicry in ovarian cancer. *Cancers (Basel)*. 2022;14:4851. [\[CrossRef\]](#)
- Bhat SM, Badiger VA, Vasishta S, et al. 3D tumor angiogenesis models: recent advances and challenges. *J Cancer Res Clin Oncol*. 2021;147:3477-3494. [\[CrossRef\]](#)
- Chong Y, Xu S, Liu T, et al. Curcumin inhibits vasculogenic mimicry via regulating ETS-1 in renal cell carcinoma. *Curr Cancer Drug Targets*. 2024;24:1031-1046. [\[CrossRef\]](#)
- Li X, Sun B, Zhao X, et al. Function of BMP4 in the formation of vasculogenic mimicry in hepatocellular carcinoma. *J Cancer*. 2020;11:2560-2571. [\[CrossRef\]](#)
- Zhou H, Yuan Y, Qian H. Expression of STAT3 and vasculogenic mimicry in gallbladder carcinoma promotes invasion and metastasis. *Exp Ther Med*. 2021;22:738. [\[CrossRef\]](#)
- Wang J, Liu Y, Zhang Y, Li X, Fang M, Qian D. Targeting exosomes enveloped EBV-miR-BART1-5p-antagomirs for NPC therapy through both anti-vasculogenic mimicry and anti-angiogenesis. *Cancer Med*. 2023;12:12608-12621. [\[CrossRef\]](#)
- Gedye C, Ailles L. Isolation and characterization of cancer stem cells in vitro. *Methods Mol Biol*. 2013;946:181-204. [\[CrossRef\]](#)
- Zhang L, Wu H, Zhang Y, Xiao X, Chu F, Zhang L. Induction of lncRNA NORAD accounts for hypoxia-induced chemoresistance and vasculogenic mimicry in colorectal cancer by sponging the miR-495-3p/ hypoxia-inducible factor-1α (HIF-1α). *Bioengineered*. 2022;13:950-962. [\[CrossRef\]](#)
- Lee SH, Golinska M, Griffiths JR. HIF-1-Independent mechanisms regulating metabolic adaptation in hypoxic cancer cells. *Cells*. 2021;10:2371. [\[CrossRef\]](#)
- Wechman SL, Emdad L, Sarkar D, Das SK, Fisher PB. Vascular mimicry: triggers, molecular interactions and in vivo models. *Adv Cancer Res*. 2020;148:27-67. [\[CrossRef\]](#)
- Ma Y, Wu T, Zhou H, et al. Canstatin represses glioma growth by inhibiting formation of VM-like structures. *Transl Neurosci*. 2021;12:309-319. [\[CrossRef\]](#)
- Zeng H, Zeng X, Wang C, et al. Combination therapy using Cel-CSO/Taxol NPs for reversing drug resistance in breast cancer through inhibiting PI3K/AKT/NF-κB/HIF-1α pathway. *Drug Deliv Transl Res*. 2025;15:992-1010. [\[CrossRef\]](#)
- Yuan X, Ma C, Li J, et al. Indirect bilirubin impairs invasion of osteosarcoma cells via inhibiting the PI3K/AKT/MMP-2 signaling pathway by suppressing intracellular ROS. *J Bone Oncol*. 2023;39:100472. [\[CrossRef\]](#)
- Wei M, Ma R, Huang S, et al. Oroxylum A increases the sensitivity of temozolamide on glioma cells by hypoxia-inducible factor 1α/hedgehog pathway under hypoxia. *J Cell Physiol*. 2019;234:17392-17404. [\[CrossRef\]](#)
- Cai L, Meng B, Jiang F, et al. Novel HIF-1α Inhibitor AMSP-30m mitigates the pathogenic cellular behaviors of hypoxia-stimulated fibroblast-like synoviocytes and alleviates collagen-induced arthritis in rats via inhibiting sonic hedgehog pathway. *Inflammation*. 2023;46:2289-2305. [\[CrossRef\]](#)
- Sun T, Bi F, Liu Z, Yang Q. TMEM119 facilitates ovarian cancer cell proliferation, invasion, and migration via the PDGFRB/PI3K/AKT signaling pathway. *J Transl Med*. 2021;19:111. [\[CrossRef\]](#)
- Zhang M, Liu Y, Yin Y, et al. UBE2S promotes the development of ovarian cancer by promoting PI3K/AKT/mTOR signaling pathway to regulate cell cycle and apoptosis. *Mol Med*. 2022;28:62. [\[CrossRef\]](#)
- Sigafoos AN, Paradise BD, Fernandez-Zapico ME. Hedgehog/GLI signaling pathway: transduction, regulation, and implications for disease. *Cancers (Basel)*. 2021;13:3410. [\[CrossRef\]](#)
- Dilower I, Niloy AJ, Kumar V, Kothari A, Lee EB, Rumi MAK. Hedgehog signaling in gonadal development and function. *Cells*. 2023;12:358. [\[CrossRef\]](#)
- Zhang J, Liu Z, Jia J. Mechanisms of smoothed regulation in Hedgehog signaling. *Cells*. 2021;10:2138. [\[CrossRef\]](#)
- Ramasubbu K, Devi Rajeswari V. A novel target approach for epithelial-mesenchymal transitioning oral squamous cell carcinoma and their involvement of PI3K/Akt/mTOR and Hedgehog signaling pathway. *Oral Oncol*. 2022;134:106119. [\[CrossRef\]](#)
- Lee D, Gimple RC, Wu X, et al. Superenhancer activation of KLHDC8A drives glioma dilation and hedgehog signaling. *J Clin Invest*. 2023;133:163592. [\[CrossRef\]](#)
- Jiang L, Liu Y, Liu M, et al. REG3A promotes proliferation and DDP resistance of ovarian cancer cells by activating the PI3K/Akt signaling pathway. *Environ Toxicol*. 2024;39:85-96. [\[CrossRef\]](#)
- Zhang H, Hu L, Cheng M, Wang Q, Hu X, Chen Q. The Hedgehog signaling pathway promotes chemotherapy resistance via multidrug resistance protein 1 in ovarian cancer. *Oncol Rep*. 2020;44:2610-2620. [\[CrossRef\]](#)
- Hu X, Xu X, Zeng X, et al. Gut microbiota dysbiosis promotes the development of epithelial ovarian cancer via regulating Hedgehog signaling pathway. *Gut Microbes*. 2023;15:2221093. [\[CrossRef\]](#)
- Dong J, Cui J, Shi X, Wang T, Liu S. Itraconazole inhibits proliferation, induces apoptosis, and reduces angiogenesis of hemangioma endothelial cells by downregulating the hedgehog signaling pathway. *Heliyon*. 2023;9:19244. [\[CrossRef\]](#)
- Huang Y, Hong W, Wei X. The molecular mechanisms and therapeutic strategies of EMT in tumor progression and metastasis. *J Hematol Oncol*. 2022;15:129. [\[CrossRef\]](#)
- Cao ZQ, Wang Z, Leng P. Aberrant N-cadherin expression in cancer. *Biomed Pharmacother*. 2019;118:109320. [\[CrossRef\]](#)
- Brock T, Boudriot E, Klawitter A, et al. The influence of VE-cadherin on adhesion and incorporation of breast cancer cells into vascular endothelium. *Int J Mol Sci*. 2021;22:6049. [\[CrossRef\]](#)
- Liu S, Ni C, Zhang D, et al. S1PR1 regulates the switch of two angiogenic modes by VE-cadherin phosphorylation in breast cancer. *Cell Death Dis*. 2019;10:200. [\[CrossRef\]](#)